Orbital
The electronic journal of chemistry

the electronic journal of chemistry

Full Paper | http://dx.doi.org/10.17807/orbital.v13i4.1607

Combined Conceptual-DFT, Quantitative MEP Analysis, and Molecular Docking Study of Benzodiazepine Analogs

Rachida Djebaili [a], Nadjib Melkemi [a], Samir Kenouche [b], Ismail Daoud [c], Mohammed Bouachrine [d,e], Halima Hazhazi [a], and Toufik Salah [a]

In the present work, a combined approach based on conceptual-DFT formalism and molecular docking simulations were performed to investigate the chemical reactivity of six Benzodiazepine analogs. Chemical reactivity descriptors derived from the conceptual DFT were determined and discussed to explain the global and local reactivity of the six studied analogs. Also, long-range interactions were studied using the quantitative analyses of molecular electrostatic potential (MEP) on van der Waals surface to identify the nucleophilic and electrophilic sites. Moreover, a statistical analysis was performed to assess the robustness of atomic charges to the basis set. The results revealed that Hirshfeld population analysis (HPA) was the most efficient for this purpose. Molecular docking simulations were performed to predict the binding affinities of the issued molecules and estimate the binding poses into four binding sites, three of them were recently discovered, located in $GABA_A$ receptor.

Graphical abstract

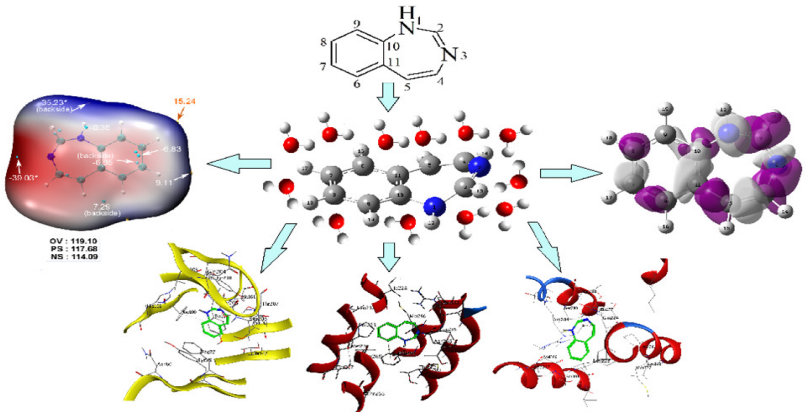

Keywords

Benzodiazepine
Binding site
Dual descriptor
Molecular docking
Quantitative MEP analysis
$GABA_A$

Article history

Received 16 March 2021
Revised 09 August 2021
Accepted 30 august 2021
Available online 26 September 2021

Handling Editor: Arlan Gonçalves

1. Introduction

The term benzodiazepines (BDZ) refer to bicyclic heterocyclic compounds based on a benzene nucleus fused to a diazepine ring. The delocalization of nitrogen atoms in the diazepine ring divided the benzodiazepines into six basic rings: 5*H*-1,2-bdz, 1*H*-1,3-bdz, 3*H*-1,4-bdz, 3*H*-1,5-bdz, 5*H*-2,3-bdz, and 1*H*-2,4-bdz (Figure 1) [1]. The classical BDZ based on

[a] Group of Computational and Pharmaceutical Chemistry, LMCE Laboratory, University Mohamed Khider, 07000 Biskra, Algeria. [b] Group of Modeling of Chemical Systems using Quantum Calculations, Applied Chemistry Laboratory (LCA). University M. Khider of Biskra, 07000 Biskra, Algeria. [c] University Abou-Bakr Belkaid-Faculty of Science- Department of Chemistry- Laboratory of Natural Substances and Bioactive (LASNABIO)-Tlemcen-Algeria. [d] MCNS Laboratory, Faculty of Science, Moulay Ismail University of Meknes, Morocco. [e] EST Khenifra, Sultan Moulay Slimane University, Morocco. *Corresponding author. E-mail: **bouachrine@gmail.com**

the structure of 3*H*-1,4-bdz are the most common psychotropic drugs that are currently marketed. They found widespread use as anxiolytics, hypnotics, muscle relaxation, and anticonvulsants in epilepsy [2, 3]. The BDZ are allosteric modulators of $GABA_A$ receptors, their pharmacological effects are exerted by the binding at the α-γ subunit interfaces in the presence of two GABA in their binding sites at α-β subunit interfaces. The GABA are neurotransmitters responsible for opening the transmembrane channel that is permeable to chloride and the presence of benzodiazepine enhances its activity, thus increasing the conduction of the chloride channel and inhibiting the excitability of neurons [4]. Recently, through their studies on $GABA_A$ receptors, J.J. Kim et al. [5] and S. Masiulis et al. [6] discovered, in addition to the classical BDZ site at the extracellular domain (ECD) α-γ interface, three new classes of BDZ binding sites in the transmembrane domain (TMD): two at α-β interfaces, and a third at the β-γ interface. This latter site may contribute to the TMD stability and may also have a role in the anesthetic behavior of BDZ.

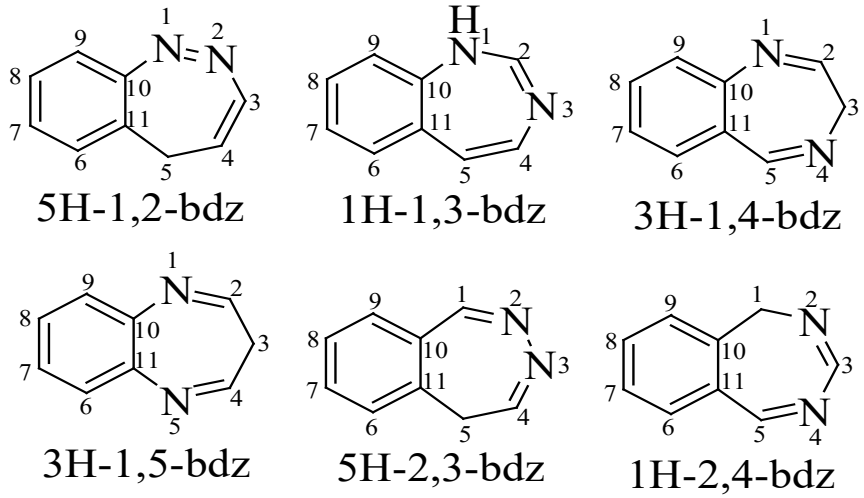

Fig. 1. The benzodiazepine basic structures.

BDZ also has wide pharmacological applications outside the central nervous system (CNS) such as anticancer [7, 8], antitrypanosomal [9, 10], non-nucleoside inhibitors of HIV-1 reverse transcriptase [11], antimicrobial agent [12, 13], antimalarial [14], antitumor agent [15], inhibitors of cholesterol absorption [16], inhibitors of the respiratory syncytial virus [17], and inhibitors of HCV NS5B polymerase [18]. Due to the broad biological applications of this class of compound, knowledge of structural parameters, electronic proprieties, and chemical reactivity of basic rings is certainly of great interest and can help in understanding the affinity of those drugs for the specific receptors. Thus the contribution in the systematization of their main therapeutic activities by modifying the old molecules or generating new substances [2, 19]. Literature revealed that there are many previous studies [1, 20–22] discussing the synthesis of different benzodiazepine derivatives with various biological activities based on modifications and substitutions to these six basic rings. However, to our knowledge, these chemical structures have not been the subject of a theoretical study.

In this paper, the four most commonly used electronic population methods in molecular modeling have been examined using statistical analysis. Global and local DFT-derived reactivity descriptors have been determined and discussed to explain the global and local reactivities of the six benzodiazepine analogs. The quantitative MEP analysis on van der Waals surface was carried out to examine the long-range intermolecular interactions. Molecular docking procedure was conducted to estimate binding affinities and binding poses in four benzodiazepine binding sites in the $GABA_A$ receptor

2. Material and Methods

2.1 Global and Local Reactivity Descriptors

Conceptual DFT-based descriptors have emerged as powerful tools for describing and analyzing the chemical reactivity and selectivity of molecular systems. Through successive derivatives of the electronic energy developed in the canonical ensemble $E[N; v(r)]$, several descriptors of reactivity have been proposed and physical meanings have emerged. The proposed global descriptors provide information on the global behavior of chemical species as a whole, and the local descriptors give a profound understanding of the reactivity of a specific atomic site in a molecule during chemical interactions [23].

Parr and Pearson [24, 25] defined the chemical hardness (η) as the second partial derivative of total energy with respect to the number of electrons:

$$\eta = (\partial^2 E/\partial N_e^2)_{v(r)} \quad (1)$$

$$\chi = -\mu = (\partial E/\partial N_e)_{v(r)} \quad (2)$$

Electronegativity (χ) is defined as the ability of chemical systems to attract electrons. The above equation implies that the concept of electronegativity appears as the opposite of chemical potential (μ) .

The reciprocal of the global hardness is defined as its global softness [26]:

$$S = 1/2\eta \quad (3)$$

On another side, the combination of global hardness (η) with the chemical potential (μ) is given by Parr et al. [27] as the electrophilic index:

$$\omega = \mu^2/2\eta \quad (4)$$

Indeed, a system with a high ω value will naturally be more prone to accepting electrons and thus be highly reactive [28]. The nucleophilic index is given by [29, 30]:

$$N = \xi_{HOMO(Nu)} - \xi_{HOMO\,(TCE)} \quad (5)$$

This nucleophilicity scale is referred to tetracyanoethylene (TCE). The latter taken as a reference because it presents the lowest HOMO energy in a large series of molecules [30]. On another side, the statement that a good nucleophile is systematically a poor electrophile or vice versa is only true for simple systems [31].

A classification scale of nucleophilicity and electrophilicity has been proposed by [30, 32]. By using the finite difference approximation, equations (1) and (2) becomes as follows:

$$\chi = -\mu = 1/2\ (A + I) \quad (6)$$

$$\eta = 1/2\ (I - A) \quad (7)$$

Where **A** is the vertical electronic affinity, defined as the quantity of energy released as a result of the capture of an electron by a neutral atom (or molecule) to form a negative ion. The property **I** is the vertical ionization potential, defined as the quantity of energy that must be supplied to a neutral atom (or molecule) to remove the most loosely bound electron and form a positive ion [33]. The equations below give the arithmetic forms of **A** and **I**:

$$A = E_N - E_{N+1} \quad (8)$$

$$I = E_{N-1} - E_N \quad (9)$$

Where, E_N, E_{N+1}, and E_{N-1} are the total ground-state energies of neutral, anionic, and cationic states, determined at the neutral geometry.

The most important local reactivity descriptor derived from conceptual DFT is the Fukui function defined according to [34, 35]:

$$f(r) = \left(\frac{\partial \rho(r)}{\partial N_e}\right)_{v(r)} = \left(\frac{\delta \mu}{\delta v(r)}\right)_{Ne} \quad (10)$$

Where μ refers to the chemical potential. High Fukui function values imply large variations in electron density and therefore the most reactive molecular sites when the number of electrons is changed. By using the finite difference approximation (FDA), the electrophilic $f^+(r)$ and nucleophilic $f^-(r)$ Fukui functions are calculated according to the formulas:

$$f^+(r) = \left(\frac{\partial \rho(r)}{\partial N_e}\right)^+_{v(r)} = \rho_{N+1}(r) - \rho_N(r) \quad (11)$$

$$f^-(r) = \left(\frac{\partial \rho(r)}{\partial N_e}\right)^-_{v(r)} = \rho_N(r) - \rho_{N-1}(r) \quad (12)$$

Where, $\rho_N(r)$, $\rho_{N-1}(r)$, and $\rho_{N+1}(r)$ are the total electronic densities at point **r** for neutral (N), cationic (N-1), and anionic (N+1) systems, respectively. In terms of the frontier molecular orbitals approximation (FMO), the Fukui functions are evaluated through the formulas:

$$f^+(r) \approx \rho_{LUMO}(r) = |\phi_{LUMO}(\vec{r})|^2 \quad (13)$$

$$f^-(r) \approx \rho_{HOMO}(r) = |\phi_{HOMO}(\vec{r})|^2 \quad (14)$$

This approximation provides a fast way to calculate the Fukui functions, but neglects the orbital relaxation effect [36]. Moreover, the condensed forms of the electrophilic and nucleophilic Fukui functions, calculated using the procedure proposed by *Yang and Mortier* [37], are given according to:

$$f^+(r) = p^k_{N+1} - p^k_N \quad (15)$$

$$f^-(r) = p^k_N - p^k_{N-1} \quad (16)$$

Where p^k_N, p^k_{N-1}, and p^k_{N+1} are the electronic populations of the k^{th} atom in the neutral, cationic, and anionic systems, respectively. The electronic population is the difference between the atomic number Z_K and the atomic charge Q_K [38]. The atomic charges can be calculated according to various population analysis schemes, as we will see in the next sections.

The dual descriptor $f^{(2)}(r)$ is another useful function used to reveal reactive sites [39, 40]. This descriptor has the advantage to locate simultaneously the electrophilic and nucleophilic sites in a volume element centered at **r**. Regions having more positive values $(f^{(2)}(r) > 0)$ are the preferred sites for nucleophilic attacks, and regions with more negative values $(f^{(2)}(r) < 0)$ are the preferred sites for electrophilic attacks. As for the Fukui functions, through the FDA and FMO approximations, this descriptor is calculated using the formulas:

$$f^{(2)}(r) = f^+(r) - f^-(r) = \rho_{N+1}(r) - 2\rho_N(r) + \rho_{N-1}(r) \quad (17)$$

$$f^{(2)}(r) \approx \rho_{LUMO}(r) - \rho_{HOMO}(r) \quad (18)$$

Other formulas have been proposed to take into account the degeneracy of the frontier orbitals [41–46].

2.2 Statistical Analysis

Before computing the condensed-to-atom reactivity descriptors; we should preliminarily determine the condensation method through the population analysis scheme. There are several schemes to achieve this objective. However, there is no consensus on which scheme is the most ideal one to study the reactive sites, through the condensed version of reactivity descriptors.

Indeed, it is difficult to choose the best electronic population analysis by referring exclusively to strictly theoretical arguments. In this study, we used a test statistic to select the most efficient method to assess the net atomic charges. The statistical quantity to be calculated for this purpose is defined according to Lebart et al. [47].

$$t_k = \frac{\bar{q}_{k,p} - \bar{q}_k}{\sqrt{\frac{S^2_k}{n_p}\left(\frac{n-n_p}{n-1}\right)}} \quad (19)$$

Where, $\bar{q}_{k,p}$ is the mean calculated for the k^{th} atom using the electronic population *p*, $\bar{q}_k$is the mean calculated for the k^{th} atom using all electronic population schemes, n_p and S_k is the number of atomic charges in the electronic population *p*, and the standard deviation of q_k estimated for the k^{th} atom using all the electronic population schemes, respectively. The p-value or critical probability is computed as follows:

$$p.value = 1 - P(|Z| < |t_k|) = 1 - \phi(|t_k|) Z \sim N\ (0,1)$$

Where, $\emptyset(|t_k|)$ is the cumulative distribution function of the standard normal distribution. The p-value is computed under the null hypothesis $(H_0: \bar{q}_{k,p} - \bar{q}_k = 0)$. Indeed, if the p-value is less than or equal to significance level 0.05 $(1 - \emptyset(|t_k| \leq 0.05)$. Then,$\bar{q}_{k,p}$ is significantly different compared to the overall mean $\bar{q}_k$. In such a case, the corresponding charge characterizes the k^{th} atom. On the other hand, the alternative hypothesis is verified if $(H_1: \bar{q}_{k,p} - \bar{q}_k \neq 0)$.

2.3 Computational Details

In order to determine the electronic properties of the benzodiazepines under study, the atomic charges were assessed using four electronic population schemes including Mulliken population analysis (MPA) [48], natural population analysis (NPA) [49], electrostatic method (ChelpG) [50], and Hirshfeld population analysis (HPA) [51]. For this purpose, the starting geometry of 3*H*-1,4-bdz (Figure 1*)* was optimized in water using six different basis sets, 6-31G, 6-311G, 6-31$^+$G (d), 6-311$^+$G (d), 6-31^{++}G (d,p), and 6-311^{++}G (d,p) in combination with the four electron population schemes. Latter, the six benzodiazepine analogs (Figure 1) were optimized in water as

neutral structures at the DFT/Ub3lyp/6-311++G(d,p) level of theory using the PCM solvation model. The molecular optimizations were performed using the Gaussian 09W software [52]. For all stationary points, there is no imaginary frequency at the optimized molecular geometries ensuring that the optimized structures are in the minimum on the potential energy surface. The atomic charges have been assessed using the Hirshfeld electronic population scheme. The singly charged anionic *(N+1)* and cationic *(N-1)* states were computed by single-point calculations at the same equilibrium geometry as the original molecule (neutral system).

The Fukui functions and the dual descriptor density mapped surfaces were visualized according to the FMO approximation. The condensed Fukui functions and the dual descriptor are calculated according to the formulas cited above. The quantitative analysis of MEP on van der Waals surface was conducted using the multifunctional wave function analyzer program Multiwfn 3.7 [53], combined with the Cubegen utility of Gaussian 09W software [52]. ESP-mapped molecular van der Waals surfaces were rendered by VMD 1.9.1program [54] based on the outputs of Multiwfn.

2.3.1 Molecular Docking Protocol

Molecular docking simulation was performed into four benzodiazepine binding sites in the $GABA_A$ receptor using Moe 2014 software package [55]. The electron microscopy structures of Human $GABA_A$ receptor alpha1-beta2-gamma2 subtypes in complex with GABA plus the diazepam (DZP) structures (PDB ID:6X3X, Resolution= 2.92 Å) were downloaded from RCSB Database (http://www.rcsb.org).

Firstly, molecular docking was carried out into the classical benzodiazepine site located between the subunits D and E. In the protein preparation step, all co-crystallized ligands and non-essential subunits (A, B, and C) have been removed from the $GABA_A$ structure to provide sterically free cavities for ligand docking. Then, after structure correction, protonation, and cavity detection, the native co-crystallized DZP structure was re-docked in the selected binding site pocket and the best pose was chosen based on the given root-mean-square deviation (RMSD) values. Finally, the six neutral benzodiazepine structures previously optimized using the DFT method were converted into database files and docked into the DZP binding site pocket.

Likewise, molecular docking was also carried out in the binding sites of the trans-membrane domain located between the subunits (A and B), (C and D), and (A and E).

3. Results and Discussion

3.1 Atomic Charges

The change in atomic charges optimized using all the basis sets are shown in Table S1, Supplementary. The performance of each electron population has been quantified by computing the ratio of critical probabilities. This performance indicator measures the robustness of each method to the basis set. The statistical results obtained are collected in Tables 1 and 2.

Table 1. The statistical test results for Mulliken and NBO populations.

Atom	Mulliken					NPA				
	t_k	$\bar{q}_{k,p}$	$\bar{q}_k$	S_k	p-value	t_k	$\bar{q}_{k,p}$	$\bar{q}_k$	S_k	p-value
1 N	1.529	-0.201	-0.372	0.221	0.063	-1.561	-0.463	-0.372	0.221	**0.059**
2 C	-2.870	0.035	0.121	0.087	**0.002**	1.567	0.144	0.121	0.087	**0.059**
3 C	-2.510	-0.379	-0.059	0.368	**0.006**	-2.178	-0.337	-0.059	0.368	**0.015**
4 N	2.431	-0.191	-0.391	0.237	**0.008**	-0.733	-0.451	-0.391	0.237	0.232
5 C	-3.692	-0.348	0.062	0.320	**0.000**	0.329	0.099	0.062	0.320	0.371
6 C	-2.868	-0.340	-0.183	0.157	**0.002**	-0.013	-0.184	-0.183	0.157	0.495
7 C	-1.177	-0.164	-0.130	0.083	0.119	-3.329	-0.225	-0.130	0.083	**0.000**
8 C	-2.659	-0.225	-0.129	0.104	**0.004**	-2.012	-0.202	-0.129	0.104	**0.022**
9 C	-2.470	-0.328	-0.211	0.136	**0.007**	-0.074	-0.215	-0.211	0.136	0.470
10 C	-3.408	-0.364	0.072	0.368	**0.000**	0.494	0.135	0.072	0.368	0.311
11 C	3.982	0.922	0.155	0.555	**0.000**	-1.570	-0.148	0.155	0.555	**0.058**
12 H	2.551	0.202	0.130	0.080	**0.005**	2.939	0.213	0.130	0.080	**0.002**
13 H	2.479	0.218	0.107	0.128	**0.007**	2.797	0.232	0.107	0.128	**0.003**
14 H	2.270	0.205	0.109	0.122	**0.012**	3.003	0.236	0.109	0.122	**0.001**
15 H	2.456	0.197	0.113	0.099	**0.007**	2.947	0.214	0.113	0.099	**0.002**
16 H	1.371	0.190	0.156	0.072	0.085	3.242	0.237	0.156	0.072	**0.001**
17 H	1.544	0.187	0.147	0.075	0.061	3.497	0.238	0.147	0.075	**0.000**
18 H	1.536	0.188	0.149	0.073	0.062	3.474	0.238	0.149	0.073	**0.000**
19 H	1.483	0.194	0.155	0.076	0.069	3.258	0.241	0.155	0.076	**0.001**

$\bar{q}_{k,p}$: Mean calculated for the k^{th}atom using the electronic population *p*.
$\bar{q}_k$: Mean calculated for the k^{th} atom using all electronic population schemes.
S_k: The standard deviation of q_k estimated for the k^{th} atom using all the electronic population schemes

Out of 19 critical probabilities P-value, the alternative hypothesis $(1 - \emptyset(|t_k| \leq 0.05)$ was verified by the following ratios: 79% (HPA), 74% (NPA and ChelpG), and 68% (MPA).

MPA seems to be the lowest-performing method, and this is not surprising as several objections to its results have been discussed in the literature [56, 57]. The drawback of MPA is that it is based on the one-particle density matrix defined through non-orthogonal atomic orbital basis sets [48]. Therefore, its sensitivity toward the basis sets is very high. This latter is evident from the data provided in Table 1, where we note that despite correlated Gaussian basis sets were used, the charges estimated using MPA are cover a wide range of values. Therefore, the MPA method is strongly affected by the used basis set.

Table 2. The statistical test results for ChelpG and Hirshfeld populations.

Atom	ChelpG					Hirshfeld				
	t_k	$\bar{q}_{k,p}$	$\bar{q}_k$	S_k	p-value	t_k	$\bar{q}_{k,p}$	$\bar{q}_k$	S_k	p-value
1 N	-3.758	-0.660	-0.372	0.221	**0.000**	2.698	-0.166	-0.372	0.221	**0.003**
2 C	4.130	0.246	0.121	0.087	**0.000**	-2.006	0.061	0.121	0.087	**0.022**
3 C	4.376	0.499	-0.059	0.368	**0.000**	0.312	-0.019	-0.059	0.368	0.377
4 N	-4.168	-0.734	-0.391	0.237	**0.000**	2.470	-0.188	-0.391	0.237	**0.007**
5 C	3.593	0.461	0.062	0.320	**0.000**	-0.230	0.037	0.062	0.320	0.409
6 C	0.128	-0.177	-0.183	0.157	0.449	2.753	-0.033	-0.183	0.157	**0.003**
7 C	1.558	-0.089	-0.130	0.083	**0.057**	3.079	-0.042	-0.130	0.083	**0.001**
8 C	1.973	-0.058	-0.129	0.104	**0.024**	2.698	-0.032	-0.129	0.104	**0.003**
9 C	-0.875	-0.253	-0.211	0.136	0.191	3.419	-0.050	-0.211	0.136	**0.000**
10 C	3.185	0.479	0.072	0.368	**0.001**	-0.270	0.037	0.072	0.368	0.393
11 C	-1.554	-0.134	0.155	0.555	**0.057**	-0.913	-0.021	0.155	0.555	0.181
12 H	-2.859	0.051	0.130	0.080	**0.002**	-2.632	0.057	0.130	0.080	**0.004**
13 H	-3.876	-0.066	0.107	0.128	**0.000**	-1.577	0.045	0.107	0.128	**0.059**
14 H	-3.813	-0.053	0.109	0.122	**0.000**	-1.590	0.047	0.109	0.122	**0.057**
15 H	-3.559	-0.009	0.113	0.099	**0.000**	-1.844	0.050	0.113	0.099	**0.033**
16 H	-0.620	0.140	0.156	0.072	0.268	-3.994	0.056	0.156	0.072	**0.000**
17 H	-1.504	0.107	0.147	0.075	**0.051**	-3.497	0.056	0.147	0.075	**0.000**
18 H	-1.418	0.113	0.149	0.073	0.078	-3.592	0.058	0.149	0.073	**0.000**
19 H	-0.704	0.136	0.155	0.076	0.241	-4.038	0.049	0.155	0.076	**0.000**

$\bar{q}_{k,p}$: Mean calculated for the k^{th}atom using the electronic population *p*.
$\bar{q}_k$: Mean calculated for the k^{th} atom using all electronic population schemes.
S_k: The standard deviation of q_k estimated for the kth atom using all the electronic population schemes

NPA and ChelpG analysis provide the same performance. Here, the charges resist better than the charges estimated using MPA. Since they seem to be independent of the used basis sets. NPA was developed to improve the problems related to the MPA method. Thus, the working base of NPA is the construction of an orthonormal set of natural atomic orbitals (NAOs) covering the non-orthogonal basis orbitals space. The occupancy weighted symmetric orthogonalization (OWSO) procedure was applied to convert the non-orthogonal atomic orbitals into the orthonormal set, where the highest occupancy orbitals are strongly preserved in form, while orbitals with negligible occupancy can be freely deformed to achieve orthogonality [49]. This feature makes NPA insensitive to the basis set quality.

ChelpG is one of the grid-based methods derived from electrostatic potentials. In which, atomic charges are adapted to reproduce the MEP at a certain number of points around the molecular species. The methods based on ESP are limited for small molecular systems with low flexibility [58]. On larger systems, it is difficult to assign charges when the atoms are far from the points where the MEP is computed. This means that the extra-molecular MEP did not accurately determine the values of the internal atomic charges. And therefore, the predicted charges become unrealistic.

The best performance is obtained by using the HPA method. The HPA values given in Table 2 are the lowest among the considered charges and cover a small range of values sometimes equal to zero. Because the HPA scheme completely neglects the effect of atomic dipole moments.

It's good for us that Hirshfeld is the best charge population to detect the electronic properties for the studied structures since our studies are heavily based on the results of Fukui indices and the dual descriptor. Hence, HPA is the ideal solution to produces a non-negative condensed Fukui function (FF) compared to MPA, NPA, and ChelpG schemes which in some cases generate negative values. The case of negative condensed FF is systematically unacceptable, except in the case where the effects of orbital relaxation are so important that redox-induced electron rearrangement occurs [59–62].

3.2 Geometry and Electronic Properties

To illustrate the differences between the structural parameters and electronic properties of BDZ structures, the bond lengths, bond angles, and dihedral angles were collected in Table S2 in Supplementary Material and revealed in Figure 2. Table 3 gives the HPA charges assigned to each atom.

Phenyl rings present a hexagonal geometry with C-C bond length and bond angles vary from (1.383 A° to 1.423 A°) and from (117.961° to 121.965°), respectively. Accordingly, the binding of the diazepine ring in C_{10} and C_{11} resulted in a slight distortion in the bond lengths and bond angles from the normal values 1.40 A° and 120°. Consequently, the planarity was also affected as indicated by the torsion angles. The diazepine rings present non-planar structures, the significant deviations out of the phenyl plan are started from the atoms numbered 1 and 5, with dihedral angles 1-10-11-6 and 9-10-11-5 vary from (-179.465° to 178.861°) and from (-48.360° to 65.764°), respectively. These distortions differ from one structure to another depending on the molecular flexibility. The bonds that have the lowest values of lengths are considered the strongest bonds in the structures and a large amount of energy is required to break them, while the weakest bonds need less energy. Here, the lowest values of bond lengths are similar between all the structures (1.27 A°). Unlike, slight differences are appeared between the lengths of weak bonds.

According to Table 3, if we exclude the results of 1*H*-1,3-bdz we note that, in all the remaining structures, the least positive charges appear over the junction atoms C_{10} or C_{11} and the high negative charges appear over the two nitrogen atoms. In another hand, hydrogens also provide important positive charges especially H_{12} in 1*H*-1,3-bdz which has the highest positive charge between all studied systems, and this due to its direct attachment to the high-electron withdrawing atom N_1.

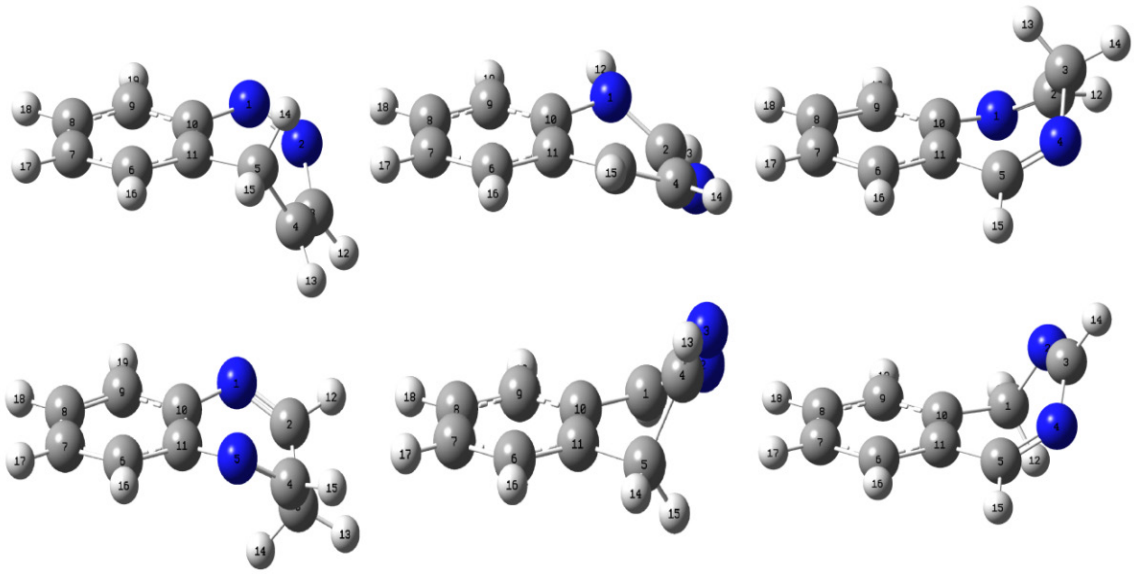

Fig. 2. Structural deformations of studied BDZ.

Table 3. Hirshfeld charges assigned to each atom, expressed in atomic units (a.u).

Atom	5*H*-1,2-bdz	1*H*-1,3-bdz	3*H*-1,4-bdz	3*H*-1,5-bdz	5*H*-2,3-bdz	1*H*-2,4-bdz
1	-0.095	-0.095	-0.163	-0.170	0.030	-0.019
2	-0.104	0.094	0.064	0.066	-0.156	-0.200
3	-0.026	-0.220	-0.020	-0.052	-0.153	0.069
4	-0.013	-0.020	-0.185	0.066	0.049	-0.179
5	-0.045	-0.067	0.039	-0.170	-0.049	0.071
6	-0.042	-0.041	-0.032	-0.055	-0.041	-0.027
7	-0.032	-0.054	-0.041	-0.045	-0.031	-0.038
8	-0.041	-0.042	-0.031	-0.045	-0.041	-0.026
9	-0.043	-0.058	-0.049	-0.055	-0.032	-0.039
10	0.011	0.042	0.038	0.022	-0.018	0.006
11	0.007	-0.023	-0.019	0.022	0.012	-0.016
12	0.052	0.141	0.055	0.056	0.051	0.038
13	0.061	0.056	0.044	0.061	0.057	0.040
14	0.047	0.038	0.045	0.054	0.057	0.044
15	0.055	0.046	0.048	0.056	0.049	0.055
16	0.053	0.050	0.054	0.043	0.054	0.057
17	0.055	0.049	0.054	0.051	0.055	0.055
18	0.054	0.052	0.056	0.051	0.053	0.056
19	0.046	0.053	0.046	0.043	0.055	0.054

Table 4. Values of HOMO-LUMO gap (Δ), global reactivity indices (*χ, η, S, ω, N*), and dipole moment (DM).

basic rings	E_{HOMO}(eV)	E_{LUMO}(eV)	Δ (eV)	A (eV)	I (eV)	χ (eV)	η (eV)	S (eV^{-1})	ω (eV)	N (eV)	DM (Debye)
5*H*-1,2-bdz	-6.460	-2.503	3.957	2.645	6.402	4.524	1.878	0.266	5.447	2.615	5.388
1*H*-1,3-bdz	-5.751	-1.858	3.893	2.031	5.644	3.837	1.807	0.277	4.076	3.323	3.742
3*H*-1,4-bdz	-6.726	-1.832	4.895	1.992	6.620	4.306	2.314	0.216	4.006	2.348	2.570
3*H*-1,5-bdz	-6.668	-1.519	5.148	1.702	6.563	4.133	2.430	0.206	3.514	2.407	3.313
5*H*-2,3-bdz	-7.004	-1.851	5.154	2.004	6.898	4.451	2.447	0.204	4.048	2.070	5.907
1*H*-2,4-bdz	-6.902	-2.229	4.673	2.371	6.793	4.582	2.211	0.226	4.749	2.172	4.688

$A = E_N - E_{N+1}$; $I = E_{N-1} - E_N$; $\Delta = |E_{HOMO} - E_{LUMO}|$; $\chi = -\mu = 1/2(A+I)$; $\eta = 1/2(I-A)$; $\delta = 1/2\eta$; $\omega = \mu^2/2\eta$

$N = E_{HOMO} - E_{HOMO\ (TCE)}$ with $E_{HOMO\ (TCE)}$ = -9.074535 eV, calculated with DFT(Ub3lyp) /6-311^{++}G (d, p)/ Hirshfeld/PCM model.

3.3 Global Reactivity

The global reactivity indices derived from the conceptual-DFT (χ, η, S, ω, N) are calculated and discussed to explain the global changes between the six benzodiazepine analogs. Table 4 summarizes the results.

The overall hardness classifies the studied systems from the most reactive to the least, as follows: 1*H*-1,3-bdz, 5*H*-1,2-bdz, 1*H*-2,4-bdz, 3*H*-1,4-bdz, 3*H*-1,5-bdz, and 5*H*-2,3-bdz. The HOMO-LUMO energy gap (Δ) confirmed the results of global hardness, where, the high kinetic stability (high Δ) is generally associated with the low chemical reactivity (high η).

The high reactivity of 1*H*-1,3-bdz is accompanied by the highest nucleophilicity (N= 3.323 eV) and the lowest electronegativity (χ =3.837 eV). Whereas, the low reactivity of 5*H*-2,3-bdz is accompanied by the lowest nucleophilicity (N=2.070 eV) and the highest polarization (DM=5.907 Debye).

Thus, the intermolecular interactions between 5*H*-2,3-bdz and the neighboring water molecules are of great importance compared to the rest of the studied systems. Using the nucleophilicity and electrophilicity scales [30, 32], the 1*H*-1,3-bdz is classified as a strong nucleophile with strong electrophilicity. While the other systems are classified as moderate nucleophiles with strong electrophilicity.

3.4 Local Reactivity and Quantitative MEP Analysis

In this section, the selectivity of atomic sites towards the approach of nucleophilic and electrophilic reactants is investigated using the dual descriptor $f^{(2)}(r)$. The numerical values are depicted in Tables 5 and 6. The numerical values of Table 6 are mapped in Figure 3 (for $f^{+}(r)$ and $f^{-}(r)$ mapped surfaces (see Figure S1 in supplementary Material) through the use of the FMO approximation. The structures are arranged and numbered in the order given in Figure 1. Regions of positive signs are depicted by purple color, and regions of negative signs are in white (Isovalue MO = 0.0015 a.u, density = 0.00040 a.u).

Our results show that the delocalization of nitrogen along the diazepine cycle leads to significant differences in local reactivity. As a result, the ability of each atom to receive nucleophilic or electrophilic attack varies from structure to another and this may explain the wide biodiversity of the benzodiazepine family. The preferred sites for nucleophilic (electrophilic) reagents are easily determined by the highest positive (negative) value of $f^{(2)}(r)$. The symmetrical behavior of 3*H*-1,5-bdz caused it to have two identical preferred electrophilic sites are C_6 and C_9, and two identical preferred nucleophilic sites C_{10} and C_{11}. In contrast, the $f^{(2)}(r)$ values around the nitrogen atoms N_1 and N_5 are close to zero (0.004), signifying that they are neither nucleophiles nor electrophiles. Thus, the possibility of attacks on these sites is relatively negligible. The same notes for hydrogens, since most of them apparent inactive towards both attacks, and this is the only observation that can be generalized to the six studied structures.

Table 5. Values of condensed Fukui Functions $f^{+}(r)$ and $f^{-}(r)$ evaluated in the terms of anionic and cationic spin-densities, respectively.

atom	5*H*-1,2-bdz		1*H*-1,3-bdz		3*H*-1,4-bdz		3*H*-1,5-bdz		5*H*-2,3-bdz		1*H*-2,4-bdz	
	$f^{+}(r)$	$f^{-}(r)$	$f^{+}(r)$	$f^{-}(r)$	$f^{+}(r)$	$f^{-}(r)$	$f^{+}(r)$	$f^{-}(r)$	$f^{+}(r)$	$f^{-}(r)$	$f^{+}(r)$	$f^{-}(r)$
1	0.278	0.346	0.028	0.206	0.038	0.237	0.114	0.118	0.185	0.044	0.010	0.040
2	0.274	0.335	0.235	0.025	0.199	0.058	0.133	0.073	0.188	0.253	0.123	0.382
3	0.007	0.079	0.048	0.115	0.023	0.033	0.032	0.016	0.032	0.260	0.051	0.013
4	0.170	0.022	0.157	0.125	0.214	0.123	0.133	0.073	0.110	0.009	0.159	0.214
5	0.014	0.005	0.118	0.138	0.070	0.015	0.114	0.118	0.011	0.009	0.257	-0.003
6	0.000	0.006	0.046	0.004	0.022	0.072	0.119	-0.012	0.027	0.067	0.092	-0.007
7	0.076	0.030	0.023	0.065	0.055	0.167	0.053	0.123	0.144	0.137	-0.008	0.093
8	-0.009	0.016	0.104	0.070	0.098	-0.023	0.053	0.123	-0.007	-0.009	0.124	0.019
9	0.065	-0.001	-0.006	0.005	-0.007	0.142	0.119	-0.012	0.114	0.106	0.000	0.024
10	0.018	0.102	0.098	0.110	0.120	0.095	0.004	0.176	0.061	0.104	0.085	0.089
11	0.061	0.044	0.077	0.106	0.106	0.039	0.004	0.176	0.071	0.002	0.047	0.078
12	0.008	0.001	0.004	0.007	0.020	0.011	0.026	0.004	0.018	0.005	0.004	0.016
13	0.016	0.011	0.023	0.005	0.006	0.006	0.010	0.001	0.010	-0.002	0.001	0.010
14	0.005	-0.001	0.017	0.007	0.004	0.005	0.026	0.007	0.002	0.001	0.012	0.006
15	0.002	0.000	0.010	0.008	0.011	0.003	0.026	0.004	0.003	-0.001	0.022	0.020
16	0.001	0.001	0.005	-0.001	0.004	0.003	0.011	-0.001	0.003	0.003	0.009	-0.001
17	0.008	0.002	0.003	0.004	0.006	0.009	0.006	0.006	0.016	0.007	0.000	0.006
18	-0.001	0.001	0.012	0.004	0.011	-0.002	0.006	0.006	0.000	-0.001	0.012	0.001
19	0.006	0.002	0.000	-0.001	0.002	0.007	0.011	-0.001	0.013	0.004	0.001	0.001

Table 6. Values of Dual descriptor $f^{(2)}(r)$ evaluated in the term of spin-density, expressed in atomic units (a.u).

atoms	5*H*-1,2-bdz	1*H*-1,3-bdz	3*H*-1,4-bdz	3*H*-1,5-bdz	5*H*-2,3-bdz	1*H*-2,4-bdz
1	-0.068	-0.177	-0.199	-0.004	0.141	-0.030
2	-0.061	0.209	0.141	0.060	-0.064	-0.259
3	-0.071	-0.067	-0.010	0.016	-0.228	0.038
4	0.148	0.032	0.091	0.060	0.100	-0.055
5	0.009	-0.020	0.055	-0.004	0.002	0.260
6	-0.006	0.043	-0.050	0.131	-0.040	0.099
7	0.047	-0.042	-0.112	-0.070	0.007	-0.101
8	-0.026	0.034	0.121	-0.070	0.002	0.104
9	0.066	-0.012	-0.150	0.131	0.008	-0.024
10	-0.084	-0.011	0.025	-0.173	-0.043	-0.004
11	0.017	-0.029	0.066	-0.173	0.069	-0.031
12	0.007	-0.003	0.008	0.022	0.013	-0.012
13	0.005	0.018	0.000	0.009	0.012	-0.008
14	0.007	0.010	-0.001	0.019	0.000	0.006
15	0.002	0.001	0.008	0.022	0.004	0.003
16	0.000	0.006	0.001	0.012	0.000	0.010
17	0.006	-0.001	-0.003	0.000	0.009	-0.006
18	-0.002	0.008	0.013	0.000	0.001	0.011
19	0.004	0.001	-0.005	0.012	0.008	0.000

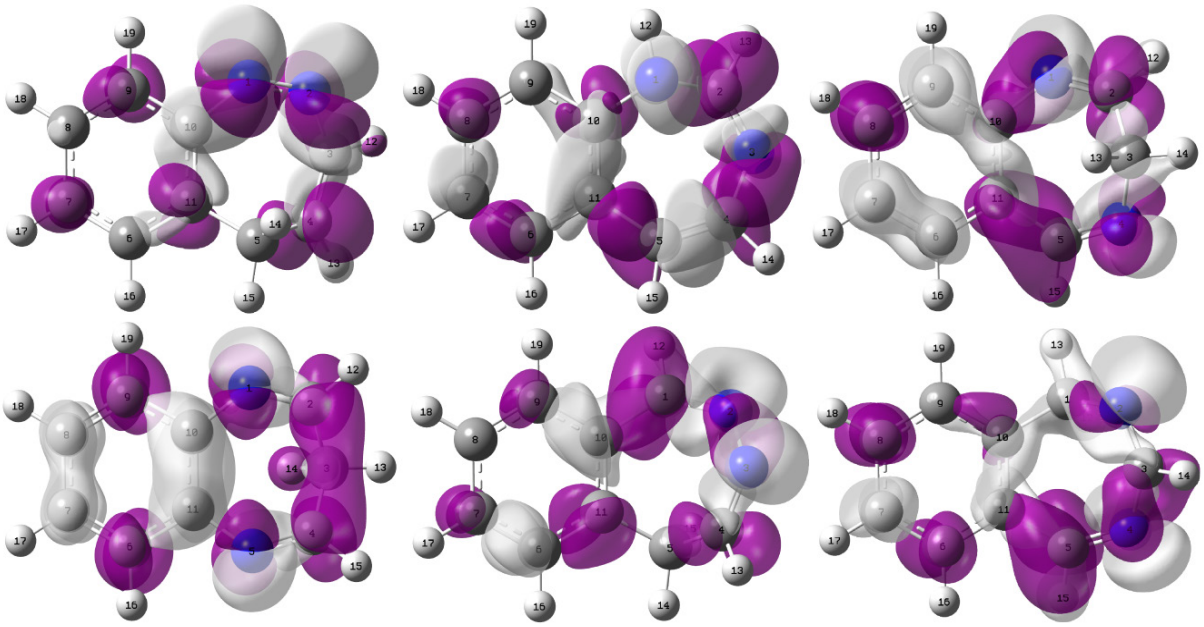

Fig. 3. Dual descriptor 3D-mapped surfaces, mapped through (FMO) approximation, Isovalue MO = 0.0015 a.u, purple color: regions of nucleophilic attacks, white color: regions of electrophilic attacks.

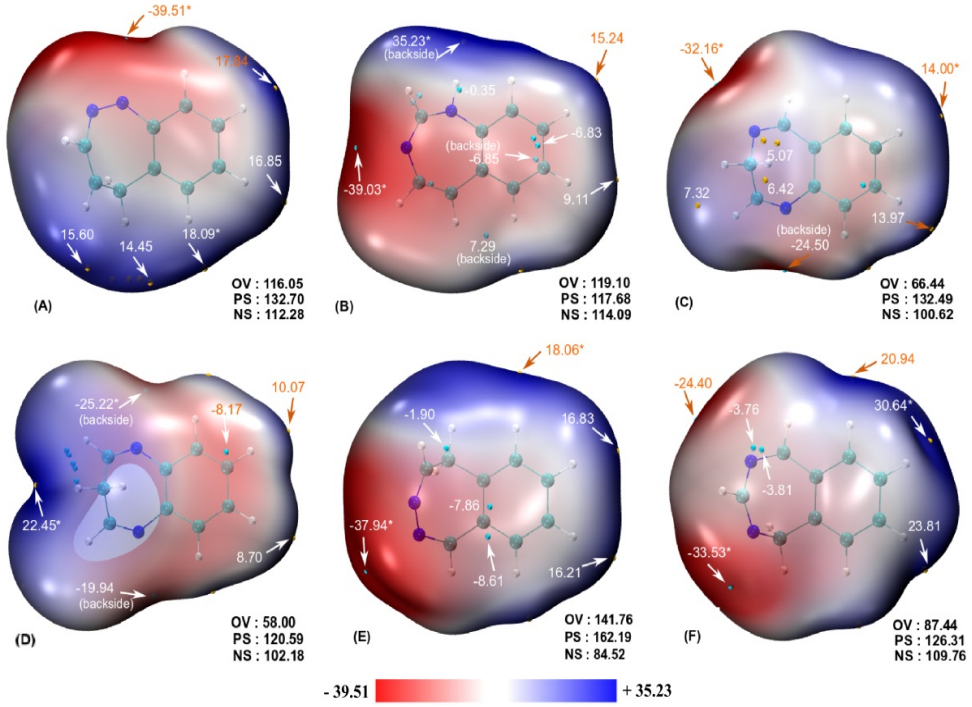

Fig. 4. ESP-mapped van der Waals surfaces (kcal/mol) using a color scale ranging fromred (negative ESP), through white (neutral ESP) to blue (positive ESP). All the iso-surface maps were rendered by VMD software based on the surface analysis result of Multiwfn program. The grid spacings were set to 0.2 *Bohr* and the van der Waals surface denotes the iso-surface of $\rho = 0.001\ a.u.$ Values with a star indicate global extremums. The bold numbers in the bottom right-hand corner are the overall ESP variance (OV), positive surface area (PS) and negative surface area (NS) whose unit are [Kcal/mol]^2, (A°)^2, respectively.

Recently, drugs based on 3*H*-1,4-bdz structure are the wide prescribed among all the benzodiazepines. The QSAR researches [63, 64] suggested that the presence of an electron-donating group in position 1, carbonyl oxygen (C=O) in position 2, phenyl group in position 5, and an electron-withdrawing group in position 7 are necessary for increasing their affinity toward the $GABA_A$ receptor. Here, we will attempt to discuss the possibility of attaching these substituents in the required positions based on the results obtained from the dual descriptor.

The values of dual descriptors suggest that N_1 and C_2 are the first privileged sites for electrophilic and nucleophilic attacks, respectively. This makes it easy to fix an electron-donating group in position 1 and a carbonyl oxygen group in position 2, using the electrophilic and nucleophilic attacks. On the other hand, the positive $f^{(2)}(r)$ value in C_5 is relatively small. Therefore, the attachment of a phenyl group in this position is possible but not much preferred since the nucleophilic attack will be directed mainly towards position 2.

Finally, our results suggest that C_7 is the third preferred nucleophilic site. Accordingly, the direct attachment of an electron-withdrawing group in this position is not recommended.

To predict the intermolecular interaction between the studied structures and the distant reagents; the quantitative MEP analysis was performed and discussed. The repulsive and attractive electrostatic interactions are long-range in comparison to the charge-transfer effects characterized by the Fukui functions and the derived reactivity indices [42]. MEP in the vicinity of a molecule is defined as the energy required to bring a unit test positive charge from infinity to the point **r**. Statistically-based molecular descriptors derived from molecular surface electrostatic potentials studied here have been defined by Politzer et al. [65].

ESP-mapped van der Waals surfaces are depicted in Figure 4. The different colors in plots representing the different values of ESP at the surface, the color code is in the range between -39.51 kcal/mol (deepest red), and 35.23 kcal/mol (deepest blue). Areas with positive ESP are electron-deficient sites and therefore subject to nucleophilic attacks, and the negative areas are electron-rich sites reacting with electrophilic reagents. The positive and negative values with a star are the global maximum and minimum ESP vdW-surface. These values indicate the most privileged sites for distant nucleophiles and electrophiles.

For more accuracy, the ESP vdW-surfaces for each atom (V_k) are given in Table 7. The atoms not mentioned in the table are having ESP values close to zero and are therefore not susceptible to any attack.

Table 7. Atomic ESP van der Waals surfaces (V_k), expressed in (kcal/mol).

atoms	5*H*-1,2-bdz	1*H*-1,3-bdz	3*H*-1,4-bdz	3*H*-1,5-bdz	5*H*-2,3-bdz	1*H*-2,4-bdz
1	-24.521	-5.471	-15.684	-15.797	-10.523	/
2	-21.236	-5.983	0.500	1.197	-24.795	-20.295
3	-4.861	-23.371	/	/	-24.869	-10.395
4	-1.742	-12.025	-18.542	1.106	-5.574	-14.107
5	/	-11.252	-1.598	-13.036	/	-1.452
6	-1.478	-7.462	-2.717	-9.884	0.146	0.083
7	-2.676	-5.653	-2.704	-9.454	-0.434	0.773
8	-4.810	-4.966	-4.173	-10.085	-1.254	-0.839
9	-7.166	-3.255	-6.106	-11.339	-2.449	-2.801
10	-6.868	-1.122	-8.442	/	-2.575	-2.929
11	-3.751	-10.793	-6.505	/	-0.099	-1.615
12	-2.064	17.254	-0.376	3.137	-2.639	-3.858
13	9.534	2.958	2.197	14.755	1.724	-3.097
14	0.044	-7.989	0.332	3.965	10.771	-8.757
15	10.592	-2.952	-3.859	3.207	2.196	1.157
16	10.494	1.219	6.267	-5.388	10.895	9.614
17	8.452	3.004	6.725	1.187	9.257	10.365
18	5.367	6.752	6.838	1.744	8.338	9.972
19	-6.724	13.767	-1.697	-5.765	5.252	4.796

The overall variance (OV) reflects the tendency of molecules to interact electrostatically with long-rang reagents. The highest OV value is 141.760 (kcal\mol)^2. This implies that the strong tendency for long-rang interactions is attributed to 5*H*-2,3-bdz, followed by 1*H*-1,3- bdz, 5*H*-1,2- bdz, 1*H*-2,4- bdz, 3*H*-1,4- bdz, and 3*H*-1,5- bdz.

If we compare this reactivity order with that given by the global hardness discussed in the global reactivity section, it is clear that both are completely identical except in the case of 5*H*-2,3-bdz where the global hardness orders it as the least reactive structure. The distribution of negative surfaces area (NS) on 5*H*-2,3-bdz and 1*H*-1,3-bdz occupy 34.3% and 49.2% of the total surfaces, respectively. This makes 5*H*-2,3-bdz have the least nucleophilic surface and 1*H*-1,3-bdz have the most nucleophilic surface among the studied systems. This result confirming the results of the global nucleophilicity indices (N) given in Table 4. Simultaneously, the positive and negative surfaces area in 1*H*-1,3-bdz have rather close values, especially when compared to the other studied systems where the negative surfaces area (NS) are significantly lower than the positive surfaces area (PS). This confirmed the classification of 1*H*-1,3-bdz as strong nucleophiles with strong electrophilicity, and the remains as moderate nucleophiles with strong electrophilicity.

According to Figure 4, each structure is surrounded by positive and negative ESP surfaces that appeared over the hydrogen atoms and the two nitrogen atoms, respectively. The highest local positive ESP values on the surfaces are appearing around: (H_{12} in 1*H*-1,3-bdz), (H_{13} in 3*H*-1,5-bdz), (H_{15} in 5*H*-1,2-bdz), (H_{16} in 5*H*-2,3-bdz), and (H_{17} in 3*H*-1,4-bdz and 1*H*-2,4-bdz), Indicating the primary favorable sites for distant nucleophiles. simultaneously, the highest local negative ESP values on the surfaces are distributed around the lone pairs of (N_1 in 5*H*-1,2-bdz and 3*H*-1,5-bdz), (N_2 in 1*H*-2,4-bdz), (N_3 in 1*H*-1,3-bdz and 5*H*-2,3-bdz), and (N_4 in 3*H*-1,4-bdz), Thus are the primary preferred sites for distant electrophiles. Also, most carbons are having negative ESP regions but less than that of the nitrogen, this negativity due to the π-electron cloud delocalization over the benzene and diazepine rings. Therefore, the possibility of electrophilic attacks in these areas is also acceptable.

3.5 Molecular Docking Simulation

The molecular docking simulation provides a direct opportunity to place the six studied structures in a biological environment and follow the interactions that arise between them and the residues of the binding sites. Moe docking was performed in four distinct benzodiazepine binding sites: the classical site at the ECD α-γ interface (labeled (a)), the two TMD sites at the α-β interfaces (labeled (b) and (c)), and the TMD site at the β-γ interface (labeled (d)) (see Figure 5). Firstly, the co-crystallized ligand diazepam (DZP) has been re-docked into the four binding sites and the best poses were chosen according to the rmsd values and visualized in Figure 6. Then, the six studied ligands have been docked into each binding site, and the best poses were selected according to the lowest energy score values.

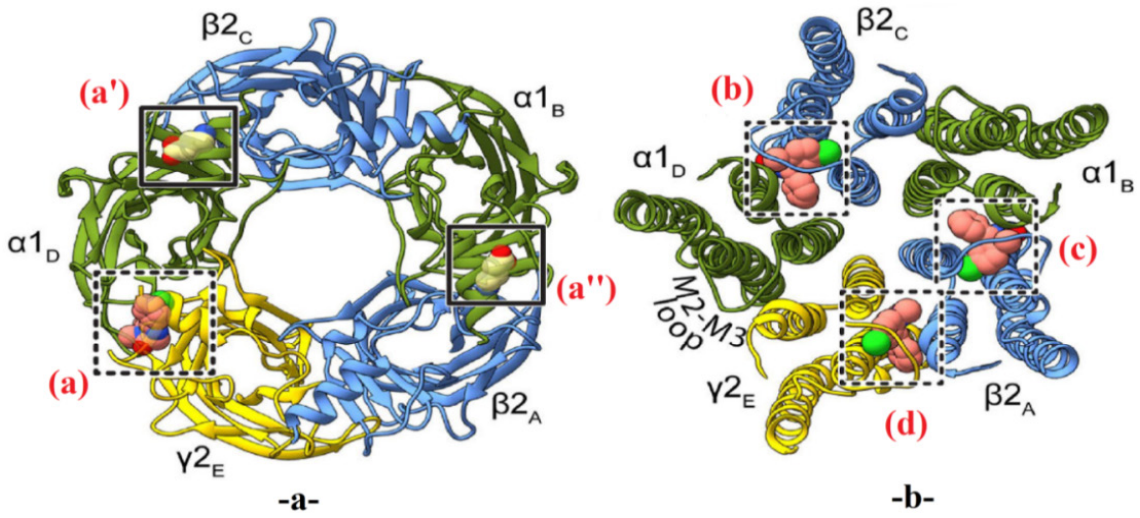

Fig. 5. -**a-**Diazepam (a) and the two GABA (a') and (a'') extracellular domain binding sites. -**b-** The three transmembrane domain binding sites (b), (c), and (d) identified for diazepam [5].

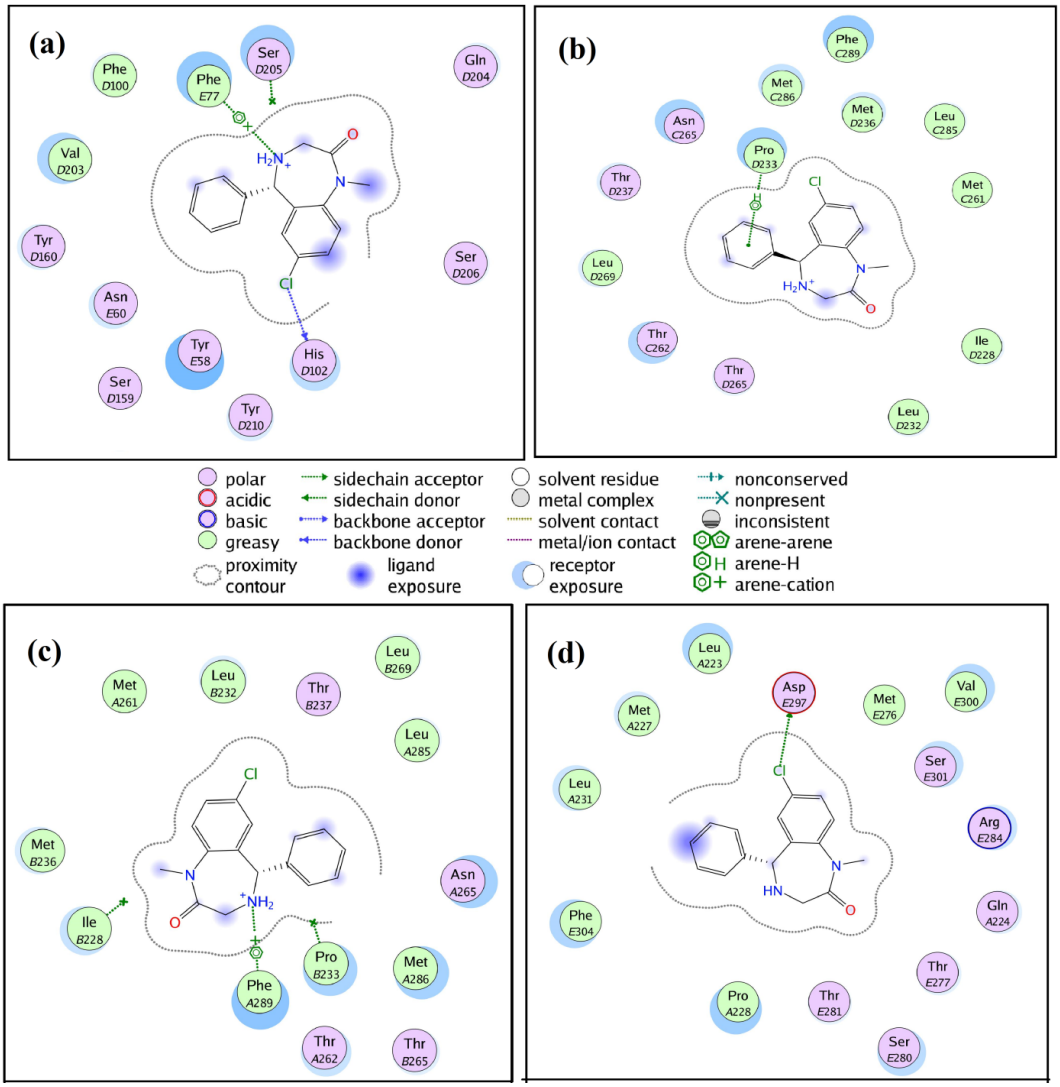

Fig. 6. The best binding poses for the re-docked co-crystallized ligand (Diazepam) in the classical site at the ECD α-γ interface (a), the two TMD sites at the α-βinterfaces (b) and (c), and the TMD site at β-γinterface (d). rmsd = 0.279, 0.357, 0.487, and 0.314, respectively.

Results such as the energy score, types, and distances of interactions between the studied ligands and the residues of the binding sites were collected in Tables 8 to 11. The docking scoring is required to quantitatively estimate the binding affinity between the target macromolecule and ligands; the best poses are those that have an energy score closer to that of the co-crystallized ligand. In the four docking results, Diazepam (DZP) gives lower energy scores than the docked

ligands, the Cl substitution in position 7 forms an average bond type H-Donor with His D102 and Asp E297 in sites (a) and (d), respectively. The π-electron cloud delocalization over the phenyl ring attached in position 5 forms a withdrawing group electrostatically attracting the hydrogen of Pro D233 in the site (b). While the interactions between the basic structure and the binding site residues are appearing only in sites (a) and (c), between the N_4 and the π-electron cloud of the phenyl ring in Phe E77 and Phe A289, respectively.

The score of binding free energy of the six docked ligands is between (-5.021 and -5.235), (-4.889 and -5.054), (-4.624 and -4.951), and (-4.479 and -4.644) for the sites (a), (b), (c), and (d), respectively. As it clear, the six ligands rather have affinities close to each other and simultaneously far from that of DZP. Despite this convergence in affinities, each ligand has a different mode of interaction with the target binding sites, and this due to the difference in ESP generated by each structure (see Figure4). This latter considered being the primary responsibility in the orientation of intermolecular interactions.

Based on the atomic ESP over the whole molecular surfaces of 1*H*-1,3-bdz given in Table 7, N_3 and H_1 would be expected to be the most acceptable sites for positive and negative distant entities, respectively. The binding poses of 1*H*-1,3-bdz mapped in Figure 7 indicate the formation of an average interaction type H-acceptor between N_3 and one of the two hydrogens of the amine group in Ala D161 of the site (a). While site (b) shows the existence of weak interaction type H-pi between H_{19} and the π-electron cloud of the phenyl ring of Phe C289. This latter can be explained by observing the orientation of ligand in the binding site, where Phe C289 seems to be further from the diazepine ring and closer to the phenyl, so, logically, Phe C289 would be interacting with the most electron-deficient site in the Phenyl ring, which is H_{19}. Sites (c) and (d) also indicate the existence of weak interactions type H-pi between the π-electron cloud of the diazepine ring and hydrogen of Arg A269 and Ser E280. This interaction does not observe in the rest studied ligands. This may be due to the strong nucleophilicity of this structure (NS occupies 49.2% of the total surface, N=3.323 eV).

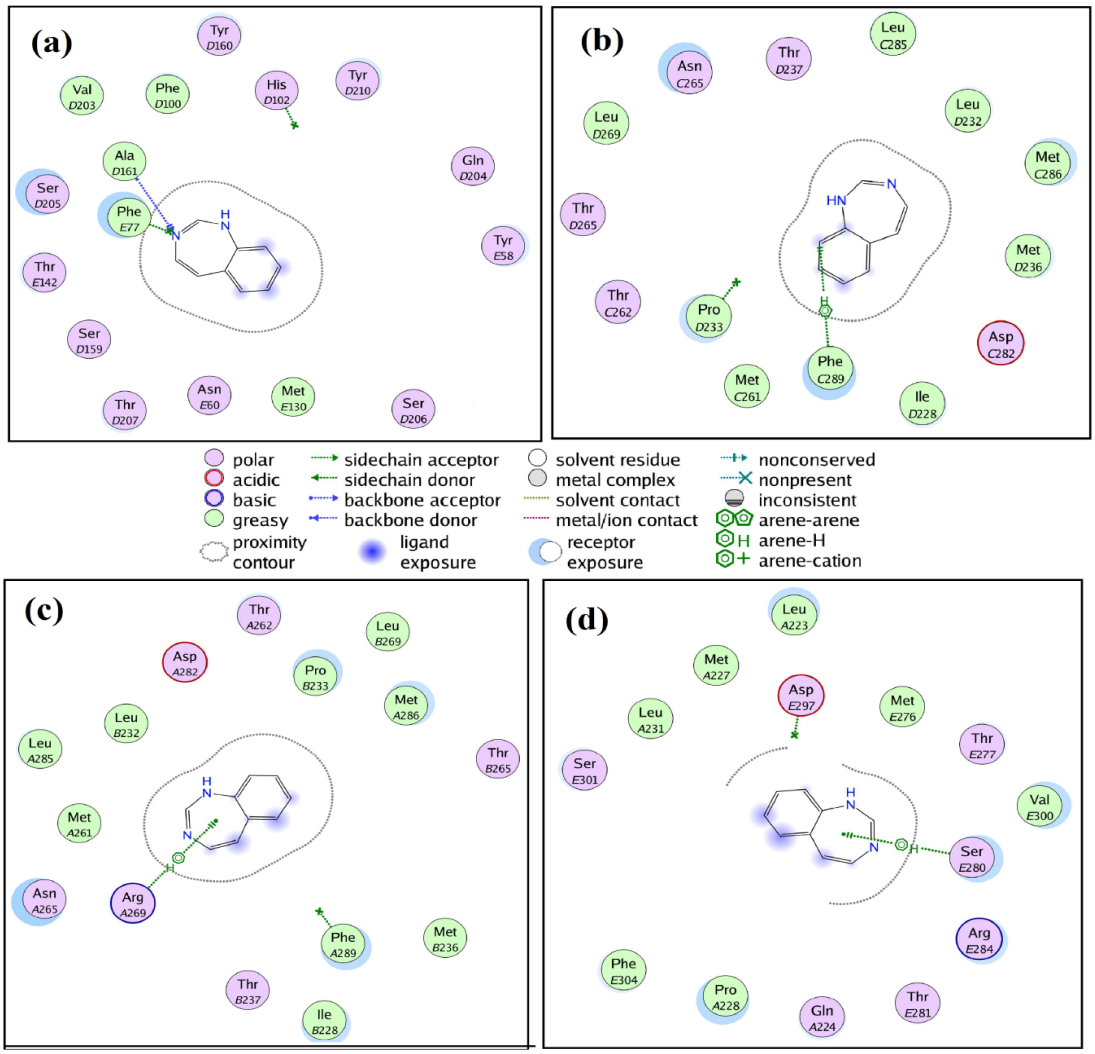

Fig. 7. The best binding poses for 1*H*-1,3-bdz ligand in the classical site at the ECD α-γ interface (a), the two TMD sites at the α-βinterfaces (b) and (c), and the TMD site at β-γinterface (d).

Similarly, the 5*H*-2,3-bdz binding poses mapped in Figure 8 indicate the formation of two strong interactions type H-acceptor between the most electron rich-site (N_3) and the two residues: Thr D207 of the site (a) and Gln A224 of the site (d). Whereas in the site (b) (see also Figure 9), the phenyl rings of 5*H*-2,3-bdz, 3*H*-1,4-bdz, and 1*H*-2,4-bdz established an arene-arene interaction with the phenyl ring of Phe C289.

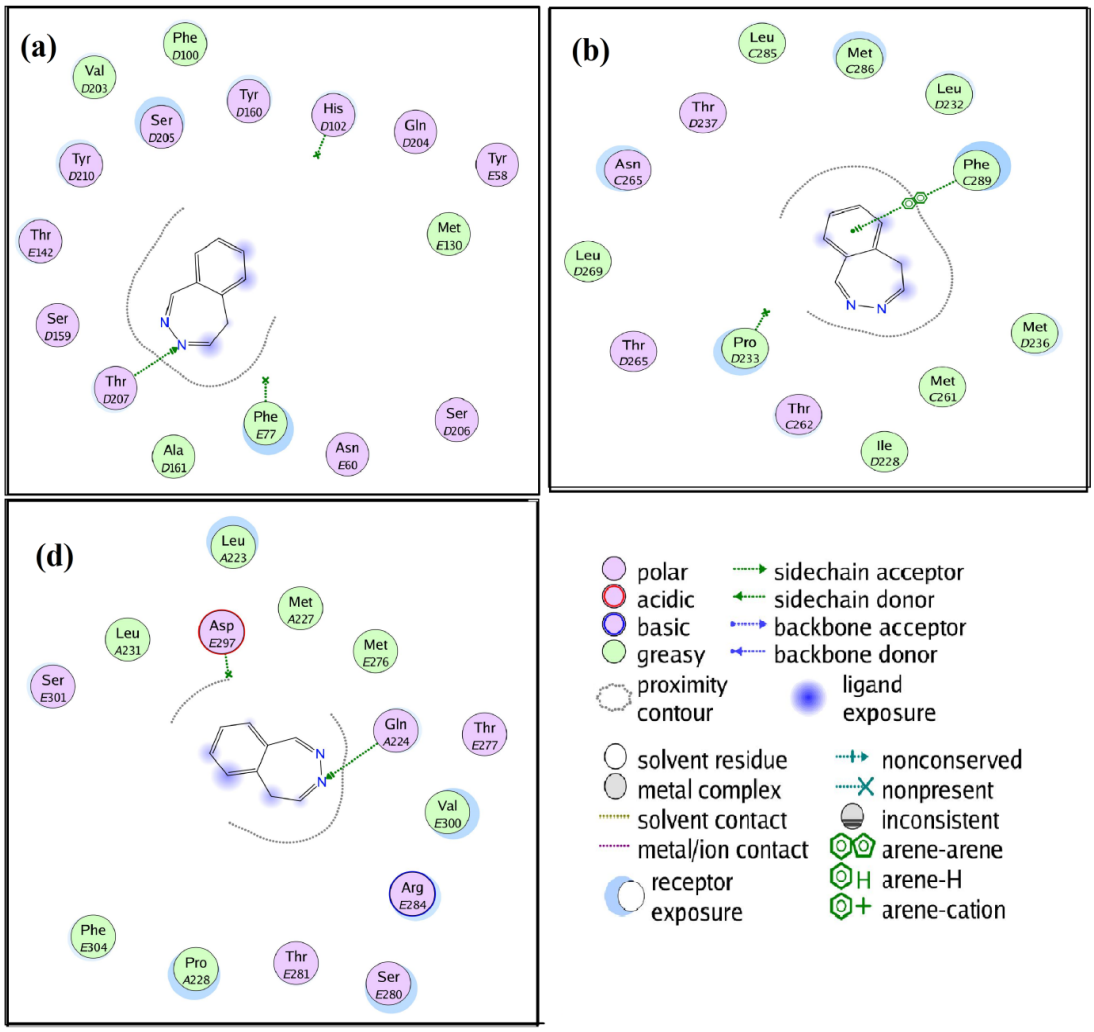

Fig. 8. The best binding poses for 5*H*-2,3-bdz ligand in the classical site at the ECD α-γ interface (a), the TMD site at the α-βinterfaces (b), and the TMD site at β-γinterface (d).

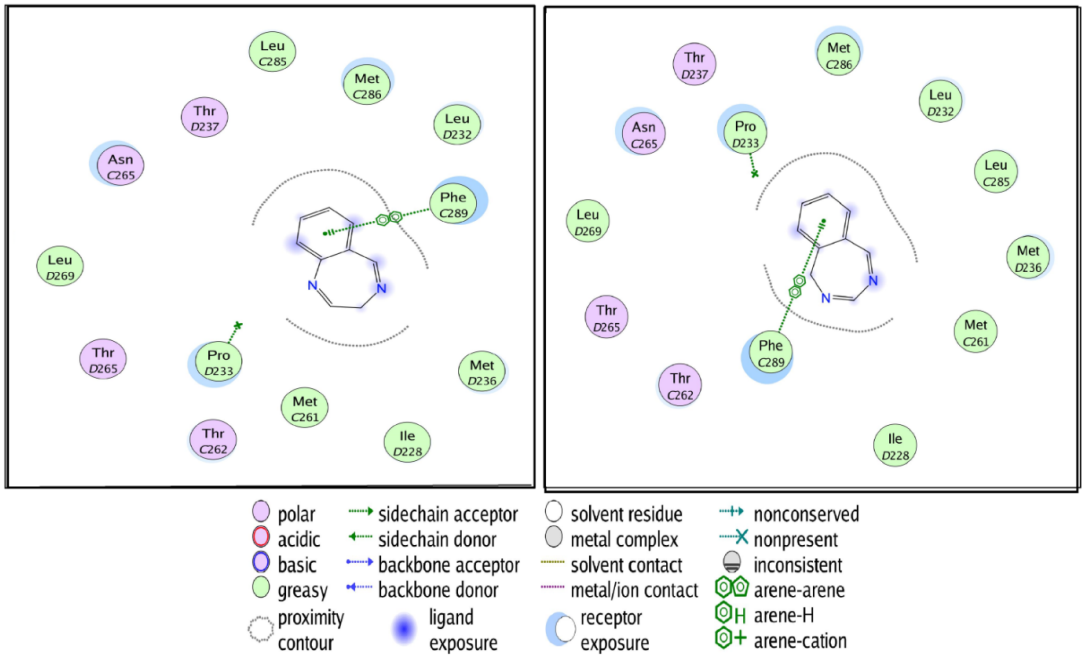

Fig. 9. The best binding poses for 3*H*-1.4-bdz and 1*H*-2,4-bdz ligands in the TMD site at the α-β interfaces (b).

Table 8. S-score, bond interactions, bond Distances, and bond energy for the Co-crystallized Ligand (Diazepam) and the six ligands docked in the classical BDZ site at the extracellular domain (ECD) α-γ interface (site (a)).

	S-score (Kcal/mol)	Atom of Ligand	Involved receptor atoms	Involved receptor residues	Type of interactions	Distances (A°)	Bond Energy (kcal/mol)
Co-crystallized Ligand							
rmsd = 0.279895216	-7.00339508	CL 36	O	HIS 102 (D)	H-donor	3.38	-1.7
		N15 23	6-ring	PHE 77 (E)	cation-pi	3.97	-2.2
Complexe $GABA_A$-ligand							
5*H*-1,2-bdz	-5.23495197	/	/	/	/	/	/
1*H*-1,3-bdz	-5.0283432	N 3	N	ALA 161 (D)	H-acceptor	3.52	-2.1
3*H*-1,4-bdz	-5.0801158	/	/	/	/	/	/
3*H*-1,5-bdz	-5.18940687	/	/	/	/	/	/
5*H*-2,3-bdz	-5.02146149	N 3	OG1	THR 207 (D)	H-acceptor	3.06	-1.0
1*H*-2,4-bdz	-5.04629469	/	/	/	/	/	/

Table 9. S-score, bond interactions, bond Distances, and bond energy for the Co-crystallized Ligand (Diazepam) and the six ligands docked in the transmembrane domain (TMD) site at the α-β interface (site (b)).

	S-score (Kcal/mol)	Atom of Ligand	Involved receptor atoms	Involved receptor residues	Type of interactions	Distances (A°)	Bond Energy (kcal/mol)
Co-crystallized Ligand							
rmsd = 0.357037723	-6.26063156	6-ring	CB	PRO 233 (D)	pi-H	3.67	-0.9
Complexe $GABA_A$-ligand							
5*H*-1,2-bdz	-5.05429792	/	/	/	/	/	/
1*H*-1,3-bdz	-4.9483633	C 9	6-ring	PHE 289 (C)	H-pi	3.80	-0.6
3*H*-1,4-bdz	-4.88927412	6-ring	6-ring	PHE 289 (C)	pi-pi	3.98	-0.0
3*H*-1,5-bdz	-4.91819811	/	/	/	/	/	/
5*H*-2,3-bdz	-4.90998173	6-ring	6-ring	PHE 289 (C)	pi-pi	3.97	-0.0
1*H*-2,4-bdz	-4.89463186	6-ring	6-ring	PHE 289 (C)	pi-pi	3.94	-0.0

Table 10. S-score, bond interactions, bond Distances, and bond energy for the Co-crystallized Ligand (Diazepam) and the six ligands docked in the transmembrane domain (TMD) site at the α-β interface (site (c)).

	S-score (Kcal/mol)	Atom of Ligand	Involved receptor atoms	Involved receptor residues	Type of interactions	Distances (A°)	Bond Energy (kcal/mol)
Co-crystallized Ligand							
rmsd = 0.487408489	-6.15904188	N15 23	6-ring	PHE 289 (A)	cation-pi	4.22	-0.7
Complexe $GABA_A$-ligand							
5*H*-1,2-bdz	-4.95116711	/	/	/	/	/	/
1*H*-1,3-bdz	-4.92590475	7-ring	CD	ARG 269 (A)	pi-H	4.73	-0.9
3*H*-1,4-bdz	-4.69323301	/	/	/	/	/	/
3*H*-1,5-bdz	-4.62413931	/	/	/	/	/	/
5*H*-2,3-bdz	-4.64065981	/	/	/	/	/	/
1*H*-2,4-bdz	-4.79273367	/	/	/	/	/	/

Table 11. S-score, bond interactions, bond Distances, and bond energy for the Co-crystallized Ligand (Diazepam) and the six ligands docked in the transmembrane domain (TMD) site at the β-γ interface (site (d)).

	S-score (Kcal/mol)	Atom of Ligand	Involved receptor atoms	Involved receptor residues	Type of interactions	Distances (A°)	Bond Energy (kcal/mol)
Co-crystallized Ligand							
rmsd = 0.314423084	-6.44459772	CL 35	OD1	ASP 297 (E)	H-donor	3.48	-0.7
Complexe $GABA_A$-ligand							
5*H*-1,2-bdz	-4.54392052	/	/	/	/	/	/
1*H*-1,3-bdz	-4.54438877	7-ring	CB	SER 280 (E)	pi-H	3.86	-1.0
3*H*-1,4-bdz	-4.64406681	/	/	/	/	/	/
3*H*-1,5-bdz	-4.63208199	/	/	/	/	/	/
5*H*-2,3-bdz	-4.47868633	N 3	NE2	GLN 224 (A)	H-acceptor	2.92	-1.3
1*H*-2,4-bdz	-4.5871954	/	/	/	/		/

4. Conclusions

In this paper, a combined approach based on conceptual-DFT theory and molecular docking simulations were performed to investigate the chemical reactivity of six Benzodiazepine analogs. Chemical reactivity descriptors derived from the conceptual DFT were determined and discussed to explain the global and local reactivity of the six studied analogs. Also, long-range interactions were studied using the quantitative analyses of the molecular electrostatic potential on van der Waals surface to identify the nucleophilic and electrophilic sites. A statistical analysis determined the robustness of each population method toward the used basis sets, the density-based method Hirshfeld presents the best performance and therefore exhibits high robustness against the basis set quality. Both global and local conceptual DFT-based descriptors were performed to provide information about global and local reactivity. The dual descriptor led to a fairly good prediction of favorable electrophilic and nucleophilic sites, making it possible to easily direct the reagents to the desired positions during the creation of new derivatives as mentioned for the 3*H*-1,4-bdz structure. The quantitative ESP analysis exhibited that the ability of each atomic site to interact electrostatically with the long-distance nucleophilic and electrophilic entities differed from structure to another. As well, the molecular docking results indicated that the six studied structures have converging binding affinities and despite this, each ligand has a different binding mode with the target sites. The interpretation of the results was given based on the quantitative analyses of ESP on van der Waals surface.

Finally, this work is an expansion to theoretical researches related to the study of heterocyclic compounds of pharmaceutical interest using DFT theory in combination with molecular docking simulation. The results obtained in this study allow deepening the understanding, from a theoretical point of view, of the chemical reactivity of six benzodiazepine basic structures. This work will certainly stimulate similar studies on a larger range of organic reactions.

Supporting Information

Table S1; Table S2; Figures S1a and S1b.

Author Contributions

Rachida Djebaili; Nadjib Melkemi, Samir Kenouche, Ismail Daoud and Toufik Salah contributed in conceptualization, methodology & investigation. Samir Kenouche and Nadjib Melkemi contributed in supervision, Formal analysis resources & software. Rachida Djebaili, Samir Kenouche, Mohammed Bouachrine, Halima Hazhazi, and Toufik Salah contributed to Writing-review & editing. All authors have read and agreed to the published version of the manuscript.

References and Notes

[1] Archer, G. A.; Sternbach, L. H. *Chem. Rev.* **1968**, *68*, 747. [Crossref]

[2] Sanger, D. J.; Benavides, J.; Perrault, G.; Morel, E.; Cohen, C.; Joly, D.; Zivkovic, B. *Neurosci. Biobehav. Rev.* **1994**, *18*, 355. [Crossref]

[3] Rudolph, U.; Knoflach, F. *Nat. Rev. Drug Discovery* **2011**, *10*, 685. [Crossref]

[4] Zhu, S.; Noviello, C. M.; Teng, J.; Walsh, R. M.; Kim, J. J.; Hibbs, R. E. *Nature* **2018**, *559*, 67. [Crossref]

[5] Kim, J. J.; Gharpure, A.; Teng, J.; Zhuang, Y.; Howard, R. J.; Zhu, S.; Noviello, C. M.; Walsh, R. M.; Lindahl, E.; Hibbs, R. E. *Nature* **2020**, *585*, 303. [Crossref]

[6] Masiulis, S.; Desai, R.; Uchański, T.; Serna Martin, I.; Laverty, D.; Karia, D.; Malinauskas, T.; Zivanov, J.; Pardon, E.; Kotecha, A.; Steyaert, J.; Miller, K. W.; Aricescu, A. R. *Nature* **2019**, *565*, 454. [Crossref]

[7] Cortes Eduardo, C.; Simon, H.-O.; Apan Teresa, R.; Camacho Antonio, N.; V. Lijanova, I.; Marcos, M.-G. *Anti-Cancer Agents Med. Chem.* **2012**, *12*, 611. [Crossref]

[8] Kamal, A.; Reddy, K. S.; Khan, M. N. A.; Shetti, R. V. C. R. N. C.; Ramaiah, M. J.; Pushpavalli, S. N. C. V. L.; Srinivas, C.; Pal-Bhadra, M.; Chourasia, M.; Sastry, G. N.; Juvekar, A.; Zingde, S.; Barkume, M. *Bioorg. Med. Chem.* **2010**, *18*, 4747. [Crossref]

[9] Maheshwari, N.; Goyal, A.; Jain, S. *Med. Chem. Res.* **2013**, *22*, 6002. [Crossref]

[10] Spencer, J.; Rathnam, R. P.; Harvey, A. L.; Clements, C. J.; Clark, R. L.; Barrett, M. P.; Wong, P. E.; Male, L.; Coles, S. J.; MacKay, S. P. *Bioorg. Med. Chem.* **2011, *19*, 1802.** [Crossref]

[11] Wiwanitkit, V. *Afr. J. Biotechnol.* **2007**, *6*, 188. [Crossref]

[12] An, Y. S.; Hao, Z. F.; Zhang, X. J.; Wang, L. Z. *Chem. Biol. Drug Des.* **2016**, *88*, 110. [Crossref]

[13] Mor, S.; Pahal, P.; Narasimhan, B. *Eur. J. Med. Chem.* **2012**, *57*, 196. [Crossref]

[14] Nallan, L.; Bauer, K. D.; Bendale, P.; Rivas, K.; Yokoyama, K.; Hornéy, C. P.; Pendyala, P. R.; Floyd, D.; Lombardo, L. J.; Williams, D. K.; Hamilton, A.; Sebti, S.; Windsor, W. T.; Weber, P. C.; Buckner, F. S.; Chakrabarti, D.; Gelb, M. H.; Van Voorhis, W. C. *J. Med. Chem.* **2005**, *48*, 3704. [Crossref]

[15] Antonow, D.; Kaliszczak, M.; Kang, G. D.; Coffils, M.; Tiberghien, A. C.; Cooper, N.; Barata, T.; Heidelberger, S.; James, C. H.; Zloh, M.; Jenkins, T. C.; Reszka, A. P.; Neidle, S.; Guichard, S. M.; Jodrell, D. I.; Hartley, J. A.; Howard, P. W.; Thurston, D. E. *J. Med. Chem.* **2010**, *53*, 2927. [Crossref]

[16] Kesäniemi, Y. A.; Miettinen, T. A. *Eur. J. Clin. Pharmacol.* **1991**, *40*, 65. [Crossref]

[17] Henderson, E. A.; Alber, D. G.; Baxter, R. C.; Bithell, S. K.; Budworth, J.; Carter, M. C.; Chubb, A.; Cockerill, G. S.; Dowdell, V. C. L.; Fraser, I. J.; Harris, R. A.; Keegan, S. J.; Kelsey, R. D.; Lumley, J. A.; Stables, J. N.; Weerasekera, N.; Wilson, L. J.; Powell, K. L. *J. Med. Chem.* **2007**, *50*, 1685. [Crossref]

[18] McGowan, D.; Nyanguile, O.; Vendeville, M. D. C. S. et al. *Bioorg. Med. Chem. Lett.* **2009**, *19*, 2492. [Crosserf]

[19] Atack, J. R. *Expert Opin. Invest. Drugs.* **2005**, *14*, 601. [Crossref]

[20] Fryer, R. I.; Bicyclic Diazepines: Diazepines with an Additional Ring, John Wiley & Sons, 2009.

[21] Aastha, P.; Navneet, K.; Anshu, A.; Pratima, S.; Dharma, K.. *Res. J. Chem. Sci.* **2013**, *3*, 90. [Crossref]

[22] Meyer, A. G.; Bissemberx, A. C.; Hyland, C. J. T.;

Charlotte C. Williams; Szabo, M.; Abel, S.-A. G.; Bird, M. J.; Hyland, I. K.; Pham, H. In: Progress in Heterocyclic Chemistry, Gribble, G. W.; Joule, J. A., eds. Elsevier, 2018, Chapter 7.

[23] Sukumar, N. *A.*; Matter of Density: Exploring the Electron Density Concept in the Chemical, Biological, and Materials Sciences, John Wiley & Sons, 2012.

[24] Pearson, R. G. *J. Chem. Educ.* **1987**, *64*, 561. [Crossref]

[25] Parr, R. G.; Pearson, R. G. *J. Am. Chem. Soc.* **1983**, *105*, 7512. [Crossref]

[26] Yang, W.; Parr, R. G. *Proc. Natl. Acad. Sci.* **1985**, *82*, 6723. [Crossref]

[27] Parr, R. G.; Szentpály, L. V.; Liu, S. *J. Am. Chem. Soc.* **1999**, *121*, 1922. [Crossref]

[28] Chamorro, E.; Chattaraj, P. K.; Fuentealba, P. *J. Phys. Chem. A.* **2003**, *107*, 7068. [Crossref]

[29] Domingo, L. R.; Chamorro, E.; Pérez, P. *J. Org. Chem.* **2008**, *73*, 4615. [Crossref]

[30] Jaramillo, P.; Domingo, L. R.; Chamorro, E.; Pérez, P. *J. Mol. Struct.: THEOCHEM.* **2008**, *865*, 68. [Crossref]

[31] Iczkowski, R. P.; Margrave, J. L. *J. Am. Chem. Soc.* **1961**, *83*, 3547. [Crossref]

[32] Domingo, L. R.; Pérez, P. *Org. Biomol. Chem.* **2013**, *11*, 4350. [Crossref]

[33] Leszczynski, J.; Handbook of Computational Chemistry, Springer Science & Business Media, 2012

[34] Fukui, K.; Yonezawa, T.; Nagata, C.; Shingu, H. *J. Chem. Phys.* **1954**, *22*, 1433. [Crossref]

[35] Fukui, K. *Science*. **1982**, *218*, 747. [Crossref]

[36] Kenouche, S.; Belkadi, A.; Djebaili, R.; Melkemi, N. *J. Mol. Graphics Modell.* **2021**, *104*, 107828. [Crossref]

[37] Yang, W.; Mortier, W. J. *J. Am. Chem. Soc.* **1986**, *108*, 5708. [Crossref]

[38] Mendoza-Huizar, L. H.; Salgado-Morán, G.; Ramirez-Tagle, R.; Glossman-Mitnik, D. *Comput. Theor. Chem.* **2016**, *1075*, 54. [Crossref]

[39] Morell, C.; Grand, A.; Toro-Labbé, A. *J. Phys. Chem. A.* **2005**, *109*, 205. [Crossref]

[40] Morell, C.; Grand, A.; Toro-Labbé, A. *Chem. Phys. Lett.* **2006**, *425*, 342. [Crossref]

[41] Martínez, J. *Chem. Phys. Lett.* **2009**, *478*, 310. [Crossref]

[42] Martínez, J. I.; Moncada, J. L.; Larenas, J. M. *J. Mol. Model.* **2010**, *16*, 1825. [Crossref]

[43] Martínez-Araya, J. I. *J. Comput. Chem.* **2016**, *37*, 2279. [Crossref]

[44] Martínez-Araya, J. I. *J. Mol. Model.* **2013**, *19*, 2811. [Crossref]

[45] Crdenas, C.; Ayers, P. W.; Cedillo, A. *J. Chem. Phys.* **2011**, *134*, 174103. [Crossref]

[46] Pino-Rios, R.; Inostroza, D.; Cárdenas-Jirón, G.; Tiznado, W. *J. Phys. Chem. A.* **2019**, *123*, 10556. [Crossref]

[47] Lebart, L.; Morineau, A.; Piron, M.; Statistique Exploratoire Multidimensionnelle, Paris: Dunod, 1995.

[48] Mulliken, R. S. *J. Chem. Phys.* **1955**, *23*, 1833. [Crossref]

[49] Reed, A. E.; Weinstock, R. B.; Weinhold, F. *J. Chem. Phys.* **1985**, *83*, 735. [Crossref]

[50] Chirlian, L. E.; Francl, M. M. *J. Comput. Chem.* **1987**, *8*, 894. [Crossref]

[51] Hirshfeld, F. L. *Theor. Chim. Acta.* **1977**, *44*, 129. [Crossref]

[52] Frisch. M. J.; Trucks, G. W.; Schlegel, H. B.; Scuseria, G. E.; Robb, M. A.; Cheeseman, J. R.; Scalmani, G.; Barone, V.; Petersson, G. A.; Nakatsuji, H.; Li, X.; Caricato, M.; Marenich, A.; Bloino, J.; Janesko, B. G.; Gomperts, R.; Mennucci, B.; Hratchian, H. P.; Ortiz, J. V.; Izmaylov, A. F.; Sonnenberg, J. L.; Williams-Young, D.; Ding, F.; Lipparini, F.; Egidi, F.; Goings, J.; Peng, B.; Petrone, A.; Henderson, T.; Ranasinghe, D.; Zakrzewski, V. G.; Gao, J.; Rega, N.; Zheng, G.; Liang, W.; Hada, M.; Ehara, M.; Toyota, K.; Fukuda, R.; Hasegawa, J.; Ishida, M.; Nakajima, T.; Honda, Y.; Kitao, O.; Nakai, H.; Vreven, T.; Throssell, K.; Montgomery, J. A.; Jr.; Peralta, J. E.; Ogliaro, F.; Bearpark, M.; Heyd, J. J.; Brothers, E.; Kudin, K. N.; Staroverov, V. N.; Keith, T.; Kobayashi, R.; Normand, J.; Raghavachari, K.; Rendell, A.; Burant, J. C.; Iyengar, S. S.; Tomasi, J.; Cossi, M.; Millam, J. M.; Klene, M.; Adamo, C.; Ca, R.; Fox, D. J. Gaussian 09W. Gaussian Inc., Wallingford CT, 2010.

[53] Lu, T.; Chen, F. *J. Mol. Graphics Modell.* **2012**, *38*, 314. [Crossref]

[54] Humphrey, W.; Dalke, A.; Schulten, K. *J. Mol. Graphics*. **1996**, *14*, 33. [Crossref]

[55] Molecular Operating Environment (MOE). Chemical Computing Group Inc.,1010 Sherbooke St. West, Suite #910, Montreal, QC, Canada, H3A 2R7, 2014 2014.

[56] Lüthi, H. P.; Ammeter, J. H.; Almlöf, J.; Faegri, K. *J. Chem. Phys.* **1982**, *77*, 2002. [Crossref]

[57] Collins, J. B.; Streitwieser, A. *J. Comput. Chem.* **1980**, *1*, 81. [Crossref]

[58] Reynolds, C. A.; Essex, J. W.; Richards, W. G. *J. Am. Chem. Soc.* **1992**, *114*, 9075. [Crossref]

[59] Roy, R. K.; Pal, S.; Hirao, K. *J. Chem. Phys.* **1999**, *110*, 8236. [Crossref]

[60] Roy, R. K.; Hirao, K.; Pal, S. *J. Chem. Phys.* **2000**, *113*, 1372. [Crossref]

[61] Roy, R. K.; Hirao, K.; Krishnamurty, S.; Pal, S. *J. Chem. Phys.* **2001**, *115*, 2901. [Crossref]

[62] Cárdenas, C.; Rabi, N.; Ayers, P. W.; Morell, C.; Jaramillo, P.; Fuentealba, P. *J. Phys. Chem. A* **2009**, *113*, 8660. [Crossref]

[63] Micheli, A.; Sperduti, A.; Starita, A.; Bianucci, A. M. *J. Chem. Inf. Comput. Sci.* **2001**, *41*, 202. [Crossref]

[64] Maddalena, D. J.; Johnston, G. A. R. *J. Med. Chem.* **1995**, *38*, 715. [Crossref]

[65] Murray, J. S.; Brinck, T.; Lane, P.; Paulsen, K.; Politzer, P. *J. Mol. Struct.: THEOCHEM.* **1994**, *307*, 55. [Crossref]

How to cite this article

Djebaili, R.; Melkemi, N.; Kenouche, S.; Daoud, I.; Bouachrine, M.; Hazhazi, H.; Salah, T. *Orbital: Electron. J. Chem.* **2021**, *13*, 301. DOI: http://dx.doi.org/10.17807/orbital.v13i4.1607